WILEY

RESEARCH ARTICLE

Neurochemical correlates of scene processing in the precuneus/posterior cingulate cortex: A multimodal fMRI and ^{1}H-MRS study

Alison G. Costigan | Katja Umla-Runge | C. John Evans | Carl J. Hodgetts | Andrew D. Lawrence | Kim S. Graham

Cardiff University Brain Research Imaging Centre, School of Psychology, Cardiff University, Wales, UK

Correspondence
Prof. Kim Graham; Cardiff University Brain Research Imaging Centre, School of Psychology, Cardiff University, Maindy Road, Cardiff, CF24 4HQ, United Kingdom.
Email: grahamks@cardiff.ac.uk

Abstract

Precuneus/posterior cingulate cortex (PCu/PCC) are key components of a midline network, activated during rest but also in tasks that involve construction of scene or situation models. Despite growing interest in PCu/PCC functional alterations in disease and disease risk, the underlying neurochemical modulators of PCu/PCC's task-evoked activity are largely unstudied. Here, a multimodal imaging approach was applied to investigate whether interindividual differences in PCu/PCC fMRI activity, elicited during perceptual discrimination of scene stimuli, were correlated with local brain metabolite levels, measured during resting-state ^{1}H-MRS. Forty healthy young adult participants completed an fMRI perceptual odd-one-out task for scenes, objects and faces. ^{1}H-MRS metabolites *N*-acetyl-aspartate (tNAA), glutamate (Glx) and γ-aminobutyric acid (GABA+) were quantified via PRESS and MEGA-PRESS scans in a PCu/PCC voxel and an occipital (OCC) control voxel. Whole brain fMRI revealed a cluster in right dorsal PCu/PCC that showed a greater BOLD response to scenes versus faces and objects. When extracted from an independently defined PCu/PCC region of interest, scene activity (vs. faces and objects and also vs. baseline) was positively correlated with PCu/PCC, but not OCC, tNAA. A voxel-wise regression analysis restricted to the PCu/PCC ^{1}H-MRS voxel area identified a significant PCu/PCC cluster, confirming the positive correlation between scene-related BOLD activity and PCu/PCC tNAA. There were no correlations between PCu/PCC activity and Glx or GABA+ levels. These results demonstrate, for the first time, that scene activity in PCu/PCC is linked to local tNAA levels, identifying a neurochemical influence on interindividual differences in the task-driven activity of a key brain hub.

KEYWORDS

default mode network, fMRI-MRS, GABA, glutamate, *N*-acetyl aspartate, posterior cingulate cortex, precuneus, scene perception

1 | INTRODUCTION

The precuneus/posterior cingulate cortex (PCu/PCC) is a key brain hub and component of a core midline system, activated during autobiographical memory, prospection, contextual retrieval, spatial navigation, and mental scene construction (Andrews-Hanna, Saxe, & Yarkoni, 2014; Bar, Aminoff, Mason, & Fenske, 2007; Buckner & Carroll, 2007;

Hassabis & Maguire, 2007; van den Heuvel & Sporns, 2013). This system substantially overlaps with the resting-state default-mode network (DMN), which is proposed to show greater activity during the resting state and deactivation during certain cognitive tasks (Fransson & Marrelec, 2008; Raichle, 2015; Raichle et al., 2001; Utevsky, Smith, & S a, 2014). However, based on its wider pattern of connectivity with medial temporal lobe (MTL) regions, including

parahippocampal and entorhinal cortices, plus the hippocampal formation (Hutchison, Culham, Everling, Flanagan, & Gallivan, 2014; Kravitz, Saleem, Baker, & Mishkin, 2011; Parvizi, Van Hoesen, Buckwalter, & Damasio, 2006; Passarelli et al., 2018), a recent proposal maintains that the PCu/PCC anchors a posteromedial or extended navigation system critical for the construction of "scene" or more generally "situation" models (comprising a particular time, place, and context; Ranganath & Ritchey, 2012). Such situation models are argued to support a diverse array of cognitive processes, including episodic memory and future thinking, spatial navigation, and scene imagination (Murray, Wise, & Graham, 2017; Ranganath & Ritchey, 2012).

In particular, it has been argued that representations of scenes or spatial contexts serve as a spatial scaffold underpinning and framing autobiographical memories and imagined events (Hassabis & Maguire, 2007; Murray et al., 2017; Robin, Buchsbaum, & Moscovitch, 2018). Consistent with this, a recent multivariate fMRI study found that the spatial context of imagined events could be uniquely decoded from activity within this posteromedial network, especially PCu/PCC (Robin et al., 2018). In addition to representing internally generated cognitive scenes or contexts, the PCu/PCC may also play a key role in representing current, external context. A situation "model" allows the viewer to construct a rich and coherent percept of a "place," extrapolating beyond the sensory input, critical both for navigation in space as well as for scaffolding episodic memories (Murray et al., 2017; Zeidman & Maguire, 2016).

Much of our knowledge of the role of PCu/PCC in scene-related cognition is based on measurements tied to neuronal activity, including blood-oxygenation-level dependent (BOLD) functional magnetic resonance imaging (fMRI) in humans (Bzdok et al., 2015; Spreng, Mar, & Kim, 2009) and single unit recording studies in both humans (Fox, Foster, Kucyi, Daitch, & Parvizi, 2018) and nonhuman primates (Dean, 2006; Sato, Sakata, Tanaka, & Taira, 2010). Further evidence comes from neuropsychological investigations of scene-based processing following brain lesions (Futamura et al., 2018; Suzuki, Yamadori, Hayakawa, & Fujii, 1998), including Alzheimer disease-linked neurodegeneration (Chan et al., 2016; Irish et al., 2015). One avenue that remains substantially unexplored is the neuro-biochemical factors underpinning PCu/PCC activity during complex scene cognition. Given the importance of this core brain hub in healthy brain function, as well as in disease (e.g., activity alterations in Alzheimer's disease and psychiatric disorders such as schizophrenia (Leech & Sharp, 2014) and in genetic risk of Alzheimer's disease (Shine, Hodgetts, Postans, Lawrence, & Graham, 2015)), improved understanding of the biochemical mechanisms underpinning the PCu/PCC fMRI response could provide useful insight into the physiological basis of its activity, which could in turn provide insight into factors underpinning activity alterations in disease and disease risk (Duncan, Wiebking, Munoz-Torres, & Northoff, 2014).

Neuro-biochemical relationships can be assessed by combining fMRI with proton magnetic resonance spectroscopy (^{1}H-MRS), as this enables the investigation of the relationship between activity and local concentrations of metabolites noninvasively *in vivo* (Duncan, Wiebking, Munoz-Torres, & Northoff, 2014; Duncan, Wiebking, & Northoff, 2014; Northoff et al., 2007). The most commonly studied ^{1}H-MRS metabolites are γ-amino-butyric acid (GABA) and

glutamate + glutamine (Glx), neurotransmitters which indicate inhibitory and excitatory tone, respectively, and *N*-acetyl-aspartate + *N*-acetyl-aspartyl-glutamate (tNAA), a neuronal marker associated with mitochondrial energy metabolism (Farrant & Nusser, 2005; Moffet, Ross, Arun, Madhavarao, & Namboodiri, 2007; Rae, 2014; Stagg & Rothman, 2014). A previous fMRI-MRS study on default-mode-related *deactivation* found that higher resting state PCu/PCC GABA+ and lower PCu/PCC Glx concentrations are associated with greater suppression of default-mode PCu/PCC activity during a working memory task (Hu, Chen, Gu, & Yang, 2013). In another study (Hao et al., 2013), higher tNAA was associated with reduced suppression of default-mode PCu/PCC activity during an auditory monitoring task. No study has yet assessed the relationship between task-driven *activation* in PCu/PCC and intrinsic regional levels of brain metabolites.

In this study, therefore, we investigated whether interindividual differences in PCu/PCC activity elicited during complex scene discrimination would be related to interindividual differences in resting state levels of PCu/PCC metabolites. An fMRI odd-one-out discrimination paradigm ("oddity"; Hodgetts et al., 2015; Shine et al., 2015) was used to investigate PCu/PCC activity in response to different stimulus categories (scenes, faces, objects). First, we hypothesised there would be a greater PCu/PCC BOLD response during scene, compared to face or object, oddity, extending previous findings of a role for PCu/PCC in complex scene cognition to involvement in online perception (Ranganath & Ritchey, 2012; Spreng et al., 2009). Second, ^{1}H-MRS metabolites were measured in the PCu/PCC region plus in a comparison region in the occipital lobe (OCC), as in Hu et al., 2013. We hypothesised a positive relationship between PCu/PCC scene-related activity and tNAA levels (consistent with Hao et al., 2013), a positive relationship between PCu/PCC scene-related activity and Glx, and a negative relationship with GABA+ (consistent with Hu et al., 2013). Finally, we predicted there would be no relationship between PCu/PCC BOLD for complex scene discrimination and OCC metabolites; a finding that would be supportive of regional specificity of any PCu/PCC BOLD-MRS relationships (Duncan, Wiebking, Munoz-Torres, & Northoff, 2014; Greenhouse, Noah, Maddock, & Ivry, 2016; Hu et al., 2013).

2 | METHODS

2.1 | Participants

Forty Cardiff University undergraduate and postgraduate students participated in this study (12 males, mean age 22.1 years, standard deviation [SD] 2.1 years, range 18.9–26.0 years). Participants were right-handed, had normal or corrected-to-normal vision, and no history of neurological or psychiatric disorders. The study received ethical approval from the Cardiff University School of Psychology Research Ethics Committee, and all participants provided written informed consent.

Due to the impact of menstrual cycle phase on ^{1}H-MRS metabolite concentrations (Batra et al., 2008; Epperson et al., 2002), scans of female participants were scheduled during their luteal phase (days 15–28 of the cycle, where Day 1 was defined as the first day of

menstruation). As GABA+ concentration does not significantly differ between pill-on and pill-free days, no restrictions were placed on scan scheduling if female participants were taking the contraceptive pill (De Bondt, De Belder, Vanhevel, Jacquemyn, & Parizel, 2015).

2.2 | Overview of experimental design

Participants completed the perceptual odd-one-out fMRI task, an anatomical MRI scan, and four ^{1}H-MRS scans within the same scan session.

2.3 | Perceptual odd-one-out ("oddity") fMRI task

The odd-one-out task was identical to that used in Shine et al. (2015) and Hodgetts et al. (2015). Participants were shown three stimuli from the same visual category on each trial and instructed to select the stimulus that was the "odd-one-out" as quickly and as accurately as possible. Four stimuli categories were used: scenes (photographs of real-world outdoor scenes, for example, parks, rivers, streets, buildings, taken by experimenters of Shine et al., 2015), faces (photographs of male and female faces, obtained from the Psychological Image Collection at Stirling (PICS; http://pics.stir.ac.uk/), objects (real-world everyday items, for example, televisions, chairs, kitchen implements, obtained from the Hemera Object Database, Vols. 1–3) or squares (taken from Barense, Henson, Lee, & Graham, 2010). For the scene, face and object categories, two of the images represented the same location, face or object, but were shown from a different viewpoint, and the third image was obtained from a visually similar, but unique, location, person, or object. The squares acted as a baseline condition, with two of the squares being of equal size, while the third square differed in size, either slightly larger or smaller. Examples of a trial from each condition are shown in Figure 1a. Participants selected the odd-one-out by pressing the corresponding button on a 3-button MRI-compatible response box, held in their right hand. The position of the correct item was counterbalanced to appear in each location an equal number of times within each condition. All images were shown only once during the task (i.e., trial-unique).

The experimental design is shown in Figure 1b. Each trial was presented for 6 s, and participants were required to make their response before the images disappeared from the screen. There was a jittered intertrial interval of 500–3,000 ms, during which participants were presented with a blank white screen. Trials were arranged into mini-blocks of three trials per stimulus category, to reduce task-switching demands. The order of mini-block categories was counterbalanced between participants.

The experiment was divided into three fMRI runs, each consisting of 72 trials, and each run lasted 11 min. Eighteen trials per stimulus category per run were presented, resulting in a total of 54 trials per condition over the three runs. The experiment was implemented using E-prime version 2.0 (Psychology Software Tools, Inc., Sharpsburg, PA). The task was viewed in a mirror mounted on top of the head coil, which allowed participants to view a projector screen (Canon Sx60 LCOS projector system combined with the Navitar SST300 zoom converter lens) located behind the scanner.

2.4 | MRI acquisition

All scans were performed at the Cardiff University Brain Research Imaging Centre (CUBRIC) on a 3 T General Electric (GE) HDx scanner fitted with an 8-channel phased array head coil. A 3D T1-weighted, fast spoiled gradient echo (FSPGR), structural MRI scan was obtained for each participant (TE/TR = 3.0/7 .9 ms; TI = 450 ms; flip angle 20°; data matrix 256 × 192 × 176; field of view 256 × 192 × 176 mm^3; acquisition time ~7 min). The FSPGR was used to aid ^{1}H-MRS voxel placement during scanning, and also as part of the subsequent fMRI and ^{1}H-MRS data analysis.

2.5 | fMRI acquisition

T2*-weighted images were acquired using a gradient-echo, echo-planar imaging (EPI) sequence (*TE/TR* = 35/3000 ms; flip angle 90°; field of view 220 mm; data matrix 64 × 64). Each of the three fMRI runs consisted of 220 volumes, with each volume comprising 42 axial slices collected in a bottom-up interleaved order. The slice thickness was 2.8 mm with an interslice gap of 1.0 mm, which created an effective voxel size of 3.8 × 3.8 × 3.8 mm^3. Slices were aligned along the anterior commissure–posterior commissure (AC–PC) line, then a 30° axial-to-coronal tilt was introduced (in the "anterior up" sense), to reduce signal dropout in the MTL caused by dephasing of the MRI signal due to nearby air-tissue and bone-tissue interfaces (Deichmann, Gottfried, Hutton, & Turner, 2003). A field map was acquired to improve registration and reduce image distortion from magnetic-field inhomogeneity (*TE*s of 7 ms and 9 ms). Each fMRI run began with four dummy volumes, to allow the signal to reach T1 equilibrium prior to acquisition.

2.6 | ^{1}H-MRS acquisition

Single voxel proton spectra were acquired from the PCu/PCC (the voxel of interest, measuring 2 × 2 × 3 cm^3), and the occipital cortex (OCC, the control voxel, measuring 3 × 3 × 3 cm^3). Examples of voxel placement and landmarks used for placement are shown in Figure 2a. The landmarks were developed through a pilot study assessing test–retest reliability of voxel placement and metabolite concentrations. To place the PCu/PCC voxel, an odd number of AC–PC aligned slices were acquired from the bottom to the top of the corpus callosum (typically 5 or 7 slices), and the middle slice was chosen (shown by "mid" black line in Figure 2a). The PCu/PCC voxel was placed on top of this line corresponding to the middle slice, and adjusted to lie posterior to the ventricles to avoid placing the voxel in an area of CSF, which could introduce artefacts to the ^{1}H-MRS spectrum. The occipital voxel was placed above the tentorium cerebelli (shown by arrow in Figure 2a) and adjusted so it did not contain any scalp tissue, which would have resulted in lipid contamination in the spectra.

In each voxel, one point-resolved spectroscopy (PRESS) scan was obtained to measure tNAA and Glx (*TE/TR* = 35/1500 ms; number of averages = 128; scan time 4 mins; Bottomley, 1984). GABA concentration (1–2 mM) is very low in comparison to the other metabolites (2–15 mM) and the peak resonances of GABA are of low amplitude due to J-coupling and are masked by the other metabolites (mainly by creatine at 3.0 ppm; Harris, Saleh, & Edden, 2017; Mullins et al., 2014). Therefore, a spectral editing acquisition (Mescher-Garwood PRESS,
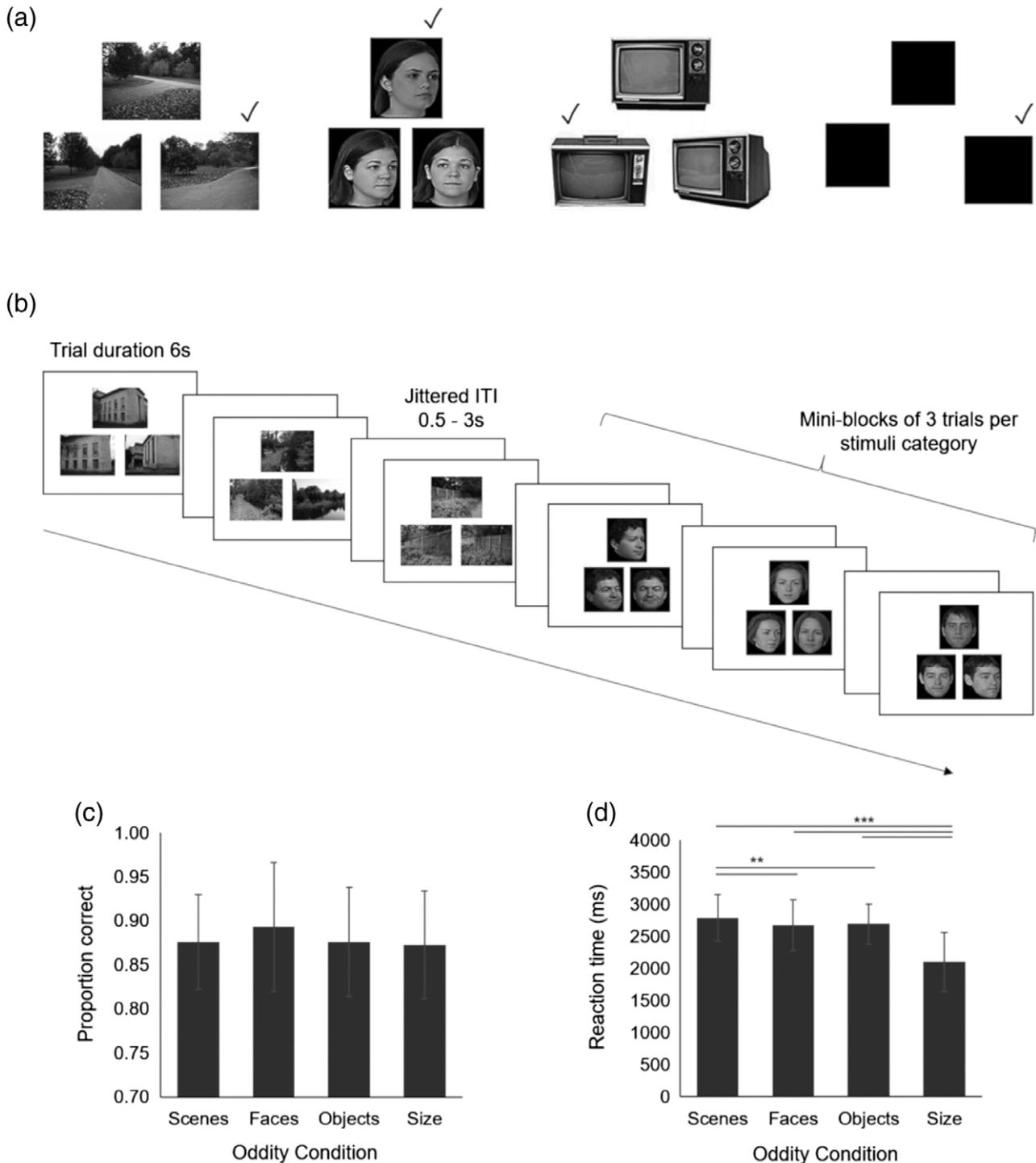
FIGURE 1 FMRI odd-one-out task. (a) Examples of a trial for each condition. Ticks indicate the correct odd-one-out. (b) Experimental design. Three trials from each category were presented in mini-blocks. Examples of a scene and face mini-block are shown. The order of mini-blocks was counterbalanced. (c and d) Behavioural results for the four stimulus categories (mean and *SE*). *N* = 35 (matched to the fMRI data shown below). (c) Proportion correct; (d) reaction time. **Indicates statistically significant at $p < 0.01$ and ***at $p < 0.001$

MEGA-PRESS; Mescher, Merkle, Kirsch, Garwood, & Gruetter, 1998) was used to alleviate the difficulties in accurately quantifying GABA. MEGA-PRESS acquisitions include additional editing pulses placed symmetrically about the water resonance (4.7 ppm) resulting in editing pulses at 1.9 ppm (edit on) and at 7.5 ppm (edit off) in order to subtract the creatine peak, enabling accurate GABA detection and quantification. One MEGA-PRESS acquisition per voxel was obtained to measure GABA + coedited macromolecules, "GABA+," (TE/TR = 68/1800 ms;

OCC 166 edit on/off pairs, scan time 10 min; PCu/PCC 256 on/off pairs, scan time 15 min [longer scan time used in smaller PCu/PCC voxel to increase signal-to-noise]). Some studies have used the edit off scan to quantify tNAA and Glx, however here we used a separate PRESS scan because short TE PRESS scans (e.g., TE 35 ms, rather than TE 68 ms as in the MEGA-PRESS edit off scan) have been found to be more accurate and repeatable at quantifying these metabolites. For example, a test–retest reliability study of PCC glutamate found that
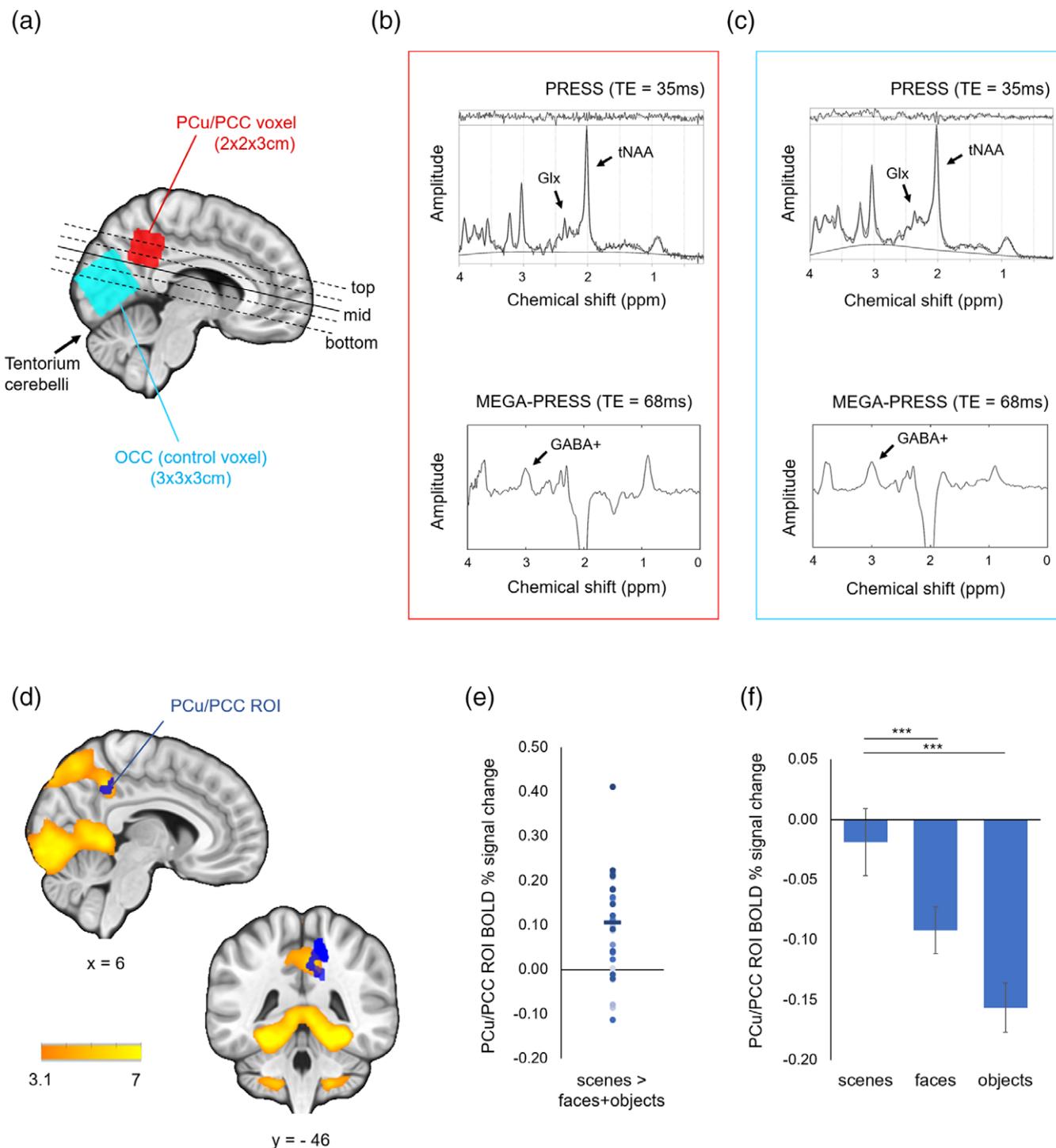
FIGURE 2 ^{1}H-MRS voxel placement and spectra and fMRI results. (a)^{1}H-MRS voxel placement for one participant. Voxels have been transformed into and overlaid on standard space. All brain data are rendered on the MNI152 2 mm standard brain template. The dotted black lines represent slices acquired from the top to bottom of the corpus callosum, which were collected to identify the mid-slice (continuous black line) to use as a landmark for PCu/PCC voxel placement. The black arrow points to the tentorium cerebelli, used as the landmark line for OCC voxel placement. (B and C) example of a PRESS and MEGA-PRESS spectrum from PCu/PCC voxel (b) and OCC voxel (c) in one participant. (d) the yellow/orange regions show the whole brain fMRI results, displaying significant clusters for the contrast of scenes > faces + objects (n = 35 participants, Z > 3.1, p < 0.05). The blue region shows the location of the a priori PCu/PCC ROI (from Shine et al., 2015), which overlaps with the PCu/PCC fMRI cluster. (e) BOLD percent signal change extracted from the a priori PCu/PCC ROI for the contrast scenes >faces + objects. Dots show each participant's BOLD percent signal change for this contrast, and horizontal lines show the mean. (f) Mean PCu/PCC ROI BOLD percent signal change for each condition relative to baseline condition of size, ± SE. ***Indicates statistically significant at p < 0.001 [Color figure can be viewed at wileyonlinelibrary.com]

over three intrascan repeats, the 35 ms PRESS scan produced a lower coefficient of variation and lower Cramer-Rao Lower Bounds (CRLBs) for Glx than PRESS scans with a longer TE (Hancu, 2009). Shimming was performed before all ^{1}H-MRS scans to ensure water-linewidth of 10 Hz or lower, in order to obtain sharp peaks in the resulting ^{1}H-MRS spectrum.

2.7 | Data analysis

2.7.1 | Behavioural data analysis

Oddity task performance was assessed by calculating the accuracy (proportion of correct odd-one-out responses) and reaction time (RT, difference between stimulus onset and button press, in milliseconds, for correct trials only) on each of the four stimulus conditions. This was calculated for each participant and each experimental run separately. Values were averaged over the three runs to obtain a mean accuracy and RT measure for each condition.

2.7.2 | fMRI data analysis

The fMRI data were preprocessed and analysed using FSL version 4.1, via the FMRI Expert Analysis Tool (FEAT; http://www.fmrib.ox.ac.uk/fsl/). Preprocessing consisted of removal of the brain from the skull via the FSL brain extraction tool (BET; Smith, 2002), motion correction using MCFLIRT (Jenkinson, Bannister, Brady, & Smith, 2002), spatial smoothing using a full-width-at-half-maximum (FWHM) Gaussian kernel of 5 mm, mean-based intensity normalisation, high pass temporal filtering set to a cut-off value of 100 s, and field map unwarping of the EPI data using FUGUE (Jenkinson, 2003).

A general linear model (GLM), consisting of four explanatory variables (the four task conditions: scenes, faces, objects, and size), was conducted for each subject and task run. An event-related design was used, and trials were modelled as 6 s events from the start of the trial presentation. Trial start times, relative to scan onset, were obtained from each participant's E-prime output file. As in previous studies, only correct trials were included in the GLMs (Hodgetts et al., 2017; Shine et al., 2015). A parameter estimate image was created for each category relative to the size baseline condition (i.e., scenes > size, faces > size and objects > size), and for the planned contrast of scenes relative to the other main stimulus categories (scenes > faces + objects). Each run was examined for participant movement and excluded if movement exceeded one fMRI voxel (>3.8 mm). This resulted in exclusion of two participants' data, and one out of the three runs for five participants. The three experimental runs for each participant (and two experimental runs for five participants) were co-registered to the Montreal Neurological Institute (MNI152) 2 mm template using FLIRT and combined using a fixed-effects model in FEAT.

To identify regions that showed a group-level preferential response to scenes compared to the other stimulus categories (scenes > faces + objects), a group-level analysis was performed using the FMRIB Local Analysis of Mixed Effects tool version 1 (FLAME 1; Beckmann, Jenkinson, & Smith, 2003; Woolrich, Behrens, Beckmann, Jenkinson, & Smith, 2004). The resulting group-averaged statistical map was thresholded with a cluster-determining threshold of $p = 0.001$ (Eklund, Nichols, & Knutsson, 2016) with a familywise error-corrected cluster threshold of $p = 0.05$ based on Gaussian random fields theory.

To obtain a quantitative measure of BOLD percent signal change in the PCu/PCC (in order to correlate with ^{1}H-MRS metabolite levels), an independently defined PCu/PCC region of interest (ROI) was used. The BOLD percent signal change in the PCu/PCC ROI for each contrast of scenes, faces and objects relative to size, and for scenes > faces + objects was extracted using the Featquery tool in FSL. The ROI chosen to sample PCu/PCC was a binarized mask of scene-related activity taken from Shine et al. (2015), which used the same fMRI paradigm, but in a different sample of individuals (peak voxel $x = 16$, $y = -46$, $z = 30$ in MNI co-ordinates, cluster size 273 voxels; see Figure 2d). A Neurosynth (Yarkoni, Poldrack, Nichols, Van Essen, & Wager, 2011) meta-analysis (http://neurosynth.org/; Database status 507,891 activations reported in 14,371 studies; 1,335 terms), revealed that the top three associations with meta-analysis maps for the peak voxel were with the terms "autobiographical" (z-score = 5.66); "default network" (z = 4.98); and "precuneus" (z = 4.9), confirming its location within the posteromedial network.

2.7.3 | ^{1}H-MRS data analysis

PRESS data were analysed using TARQUIN (Totally Automatic Robust Quantification In NMR) version 4.3.3 (Wilson, Reynolds, R a, Arvanitis, & Peet, 2011). Since it is difficult to accurately separate the peak of NAA at 2.01 ppm from that of N-acetyl-aspartyl-glutamate (NAAG) at 2.04 ppm, these were combined to create a "total NAA" or tNAA measure (NAA + NAAG; Rae, 2014). Similarly, it is difficult to accurately distinguish the spectra of glutamate and glutamine due to their largely overlapping resonances, so these measures were combined to create a composite glutamine + glutamate measure, or "Glx" (Rae, 2014; Stagg & Rothman, 2014). To ensure good quality data, metabolites were excluded if the CRLB was above 20%, consistent with the exclusion criteria commonly found in the ^{1}H-MRS literature (Cavassila, Deval, Huegen, van Ormondt, & Graveron-Demilly, 2001; Hu et al., 2013; Stagg & Rothman, 2014). This resulted in the exclusion of two PCu/PCC tNAA, three PCu/PCC Glx, one OCC tNAA and one OCC Glx measurements.

MEGA-PRESS data were analysed using GANNET (GABA-MRS Analysis Tool) version 2.0 (Edden, Puts, Harris, Barker, & Evans, 2014). The GABA concentration measured in the MEGA-PRESS scans represents GABA plus co-edited macromolecules, and is referred to as "GABA+" (Mullins et al., 2014). Data quality was assessed by two raters (authors AGC and CJE) using a 3-point rating scale (as in Lipp et al., 2015). Ratings were done blind to the fMRI results. Based on this, 11 PCu/PCC GABA+ and one OCC GABA+ measurements were excluded, considered by the raters to be poor quality data-sets.

All metabolite concentrations were corrected for voxel composition: in each participant's native space, PCu/PCC and OCC ^{1}H-MRS voxels were segmented using the FAST tool in FSL to obtain a value for the proportion of cerebrospinal fluid (CSF), grey matter (GM), and white matter (WM; Zhang, Brady, & Smith, 2001). All metabolites were quantified using H_2O as an internal concentration reference and are expressed as a concentration in millimoles (mM) per unit tissue volume. The metabolite signals were corrected to account for the CSF fraction of the voxel (due to the negligible metabolite concentration within CSF) and the water reference signal was corrected to account for the differing water content of CSF, GM, and WM (as in Harris, Puts, & Edden, 2015; Harris et al., 2015; Lipp et al., 2015).

2.8 | Statistical analysis

2.8.1 | fMRI

A repeated-measures ANOVA, implemented in SPSS version 20 (SPSS Inc., Chicago, IL), was used to assess whether the PCu/PCC ROI percent signal change for the contrasts scenes > size, faces > size and objects > size were significantly different from each other. Greenhouse–Geisser correction was used where the assumption of sphericity was not met.

2.8.2 | fMRI-MRS

Since there is no well-established benchmark method of testing the relationship between BOLD and ^{1}H-MRS metabolites (for example, see Harris et al., 2015 for five different analysis strategies), two complementary methods for assessing this relationship were implemented, consistent with Enzi et al. (2012) and Lipp et al. (2015):

Pearson correlation of ^{1}H-MRS metabolites and PCu/PCC ROI BOLD

Pearson correlations were used to assess the relationship between the BOLD response constrained to the independently defined fMRI ROI in the PCu/PCC for the contrast scenes > faces + objects and resting state tNAA, Glx, and GABA+ concentrations quantified from the PCu/PCC ^{1}H-MRS voxel. The independently defined ROI was chosen as it gives an unbiased estimate of effect size (Kriegeskorte, Simmons, Bellgowan, & Baker, 2009), and is a smaller region than the large MRS voxel (fMRI ROI volume 2184 mm^3, PCu/PCC MRS voxel volume 12,000 mm^3; as per Enzi et al., 2012). To assess the regional selectivity of any identified relationship (see Duncan et al., 2014), Pearson correlations were performed between PCu/PCC ROI BOLD for scenes > faces + objects and OCC tNAA, Glx and GABA+. In total, this created two families of three correlations (one family of interest and one control family). Bonferroni correction was applied within each family (i.e., family-wise error correction: 0.05/3 = p 0.017). This provided correction for multiple comparisons, while avoiding an overly stringent Bonferroni correction, which would have had the potential for a high risk of false negative results (Nakagawa, 2004; also see http://daniellakens.blogspot.co.uk/2016/02/why-you-dont-need-to-adjust-you-alpha.html). All statistical tests were performed using SPSS version 20 (SPSS Inc.).

To test whether correlations between PCu/PCC BOLD and metabolite concentrations in the PCu/PCC and OCC voxels were statistically different from each other, a directional Olkin's Z test, testing if the correlation with PCu/PCC tNAA was stronger than OCC tNAA, was performed as implemented in the "cocor" R package (Diedenhofen & Musch, 2015; http://comparingcorrelations.org).

As recommended by Dienes and Mclatchie (2018), Default Bayes factors (and 95% Bayesian credibility intervals) were also computed for all BOLD-MRS correlations, using JASP version 0.8.1.12 (https://jasp-stats.org/). The Bayes factor (BF) grades, on a continuous scale, the strength of the evidence that the data provide either for the alternative hypothesis (H1) versus the null (H0) expressed as BF_{10}, or for the null hypothesis versus the alternative hypothesis expressed as BF_{01} (Jarosz & Wiley, 2014; Wetzels & Wagenmakers, 2012). A BF_{10}

or BF_{01} of 1 indicates that the observed finding is equally likely under H0 and H1. A BF_{10} much greater than 1 allows us to conclude that there is substantial evidence for H1 over H0. BF_{10} values substantially less than 1 provide strong evidence in favour of H0 over H1. Conversely a BF_{01} of much greater than 1 indicates there is strong evidence in favour of H0 over H1, whereas a BF_{01} of much less than 1 indicates strong support for H1 rather than H0. Where the Pearson correlations were significant, directional BFs for these correlations were expressed as BF_{+0} in favour of a positive correlation, or BF_{-0} for a negative correlation (Marsman & Wagenmakers, 2017). Where the Pearson correlations were nonsignificant, BF_{01} in favour of the null (zero) correlation were computed.

An additional analysis was conducted post hoc to examine any association between OCC tNAA or GABA+ and OCC scene-related BOLD response. To create an independently defined OCC ROI, we used a neurosynth meta-analysis using the search term "navigation" (scene is not a search term in neurosynth). This revealed a significant voxel cluster in early visual cortex, peak (−2, −92, 22), z = 5.38. A 10 mm radius spherical ROI centred on these coordinates was created, and the BOLD percent signal change for the positive contrast scenes > size was extracted from this ROI. Pearson correlations were then performed between OCC ROI BOLD for scenes > size and OCC tNAA or GABA+.

Voxel-wise GLM using ^{1}H-MRS as a regressor

Three GLMs were created for the contrast of scenes > faces + objects, where each model included de-meaned values of either PCu/PCC tNAA, Glx or GABA+ concentrations as a regressor. These analyses were restricted to a group PCu/PCC ^{1}H-MRS voxel mask area (as in Enzi et al., 2012). Contrasts were set up so that results would show any voxels within this group mask that were positively or negatively correlated with concentrations of each metabolite. The group PCu/PCC ^{1}H-MRS voxel mask was created in MNI space by combining all participants' PCu/PCC MRS voxel masks, such that any MNI voxel present in any participant's MRS voxel mask would be included in the group voxel mask (see Figure 5 for tNAA mask). The number of participants used to create the group masks differed for the tNAA, Glx, and GABA+ analyses, as there were different numbers of participants remaining for these analyses after exclusions following data quality control (tNAA n = 33, Glx n = 32, GABA+ n = 24).

The statistical threshold for the fMRI analysis was voxel-wise, uncorrected at p < 0.01 (as in Hodgetts et al., 2015). To prevent false positives due to multiple-comparisons (as there were approximately 4,000 fMRI voxels within each PCu/PCC MRS metabolite group mask), Monte-Carlo simulation was used to determine whether the size of any resulting cluster was statistically significant, using the 3dClustSim command in AFNI (2016 version, in which the bug identified in Eklund et al. (2016) had been fixed, https://afni.nimh.nih.gov/pub/dist/doc/program_help/3dClustSim.html). A cluster-corrected threshold of p < 0.01 was selected (as in Hodgetts et al., 2015), which determined that any cluster larger than 42 voxels was statistically significant at p < 0.01 for the tNAA mask and Glx mask, and 40 voxels for the GABA+ mask.

TABLE 1 Whole brain fMRI results

Cluster number	Cluster size (voxels)	Brain region for local maxima	Hemisphere	Z value	MNI co-ordinates of peak voxel		
					x	y	z
1	25,603	Temporal occipital fusiform cortex/lingual gyrus	Right	8.81	30	−48	−12
		Temporal occipital fusiform cortex/lingual gyrus	Right	8.69	30	−52	−12
		Temporal occipital fusiform cortex/lingual gyrus	Left	8.59	−28	−52	−10
		Precuneus/intracalcarine cortex/lingual gyrus	Left	8.58	−14	−60	6
		Lingual gyrus/Precuneus	Right	8.47	18	−54	4
		Posterior temporal fusiform cortex/temporal occipital fusiform cortex	Left	8.41	−26	−42	−16
		Precuneus/posterior cingulate cortex	Right	6.34	6	−46	42
2	329	Superior/middle frontal gyrus	Right	4.71	28	2	60
3	317	Superior/middle frontal gyrus	Left	4.47	−28	8	54

Clusters that showed significantly greater activity for the contrast of scenes >faces + objects (Z > 3.1, p < 0.05). Brain region labels were defined using the Harvard-cortical atlas tool in FSL. Most regions identified are part of one large cluster; the local maxima within this cluster are listed.

3 | RESULTS

3.1 | Behaviour

There were no significant differences in the proportion of correct responses between the four conditions of the oddity task ($F[3,102] = 1.16$, $p = 0.33$, $\eta^2_p = 0.09$), suggesting that task difficulty was matched across conditions (see Figure 1c). There was, however, a significant effect of condition on RT ($F[3,102] = 97.25$, $p = 8.46 \times 10^{-30}$, $\eta^2_p = 0.86$). Posthoc tests revealed RTs were faster for the baseline condition of size than for scenes, face and objects (respectively: $t[34] = 14.34$, $p = 5.64 \times 10^{-16}$, Cohen's $d_{av} = 1.65$; $t[34] = 11.13$, $p = 7.07 \times 10^{-13}$, Cohen's $d_{av} = 1.32$ and $t[34] = 11.71$, $p = 1.75 \times 10^{-13}$, Cohen's $d_{av} = 1.50$). RTs were also slightly slower for scenes than for faces or objects respectively (scenes: $t[34] = 3.02$, $p = 0.005$, Cohen's $d_{av} = 0.30$; faces: $t[34] = 2.83$, $p = 0.008$, Cohen's $d_{av} = 0.29$; see Figure 1c). There were no significant correlations between scene discrimination performance and either PCC metabolites or PCC scene-related BOLD (data not reported).

3.2 | fMRI

3.2.1 | Whole brain results: PCu/PCC shows a greater BOLD response for scenes than faces and objects

The final fMRI sample size was 35, following exclusions due to scanner errors ($n = 3$) and movement ($n = 2 + \frac{1}{3}$ of runs excluded for five participants). Figure 2d shows the whole brain activation map for the contrast of scenes compared to faces and objects. There was a significantly greater BOLD response in the PCu/PCC region for scenes > faces + objects, suggesting this region has relative scene selectivity (peak activation in MNI co-ordinates $x = 6$, $y = −46$, $z = 42$).

Significant clusters were also identified for this contrast bilaterally in the parahippocampal gyrus, the medial portion of the hippocampus, lateral occipital sulcus, lingual gyrus, inferior regions of the precuneus, temporal occipital fusiform cortex, and occipital pole (see Figure 2d and Table 1), consistent with previous studies of scene-related activity (Hodgetts et al., 2017; Hodgetts, Shine, Lawrence, Downing, & Graham, 2016; Lee, Scahill, & Graham, 2008).

3.2.2 | PCu/PCC ROI results: Greater BOLD percent signal change in ROI for scenes than faces or objects

The a priori PCu/PCC ROI overlapped with the PCu/PCC cluster identified in the whole brain analysis (see Figure 2d). Consistent with the whole brain findings, within the PCu/PCC ROI there was significantly greater activity for scenes > faces + objects (see Figure 2e for interindividual variability in values). In support of this, when each condition was contrasted to the baseline condition of size, a repeated-measures ANOVA determined there was a significant effect of oddity condition on the BOLD percent signal change measured in the PCu/PCC ROI ($F[1.42, 48.21] = 34.68$, $p = 1.6 \times 10^{-8}$, $\eta^2_p = 0.51$ (Greenhouse–Geisser corrected degrees of freedom)). Planned comparisons confirmed that this reflected significantly higher PCu/PCC activity for scenes compared to the face and object conditions when contrasted with size: scenes > size versus faces > size ($F[1, 34] = 14.92$, $p = 4.8 \times 10^{-4}$, $\eta^2_p = 0.31$), and scenes > size versus objects > size ($F[1, 34] = 52.65$, $p = 2.1 \times 10^{-8}$, $\eta^2_p = 0.61$; see Figure 2f).

3.3 | ^{1}H-MRS

Figure 2a shows a representative PCu/PCC and OCC voxel placement. Figure 2b,c show examples of each type of spectra obtained in

TABLE 2 ^{1}H-MRS results

	PCu/PCC voxel			OCC voxel		
	tNAA	Glx	GABA+	tNAA	Glx	GABA+
Sample size (from original n = 40)	33	32	24	34	34	34
Mean concentration (mM)	16.39	20.93	1.85	13.42	21.64	1.97
SD	0.90	2.87	0.27	1.40	2.75	0.19

Sample sizes given are those after data has been removed due to scanner errors, fMRI data quality assessment, and ^{1}H-MRS quality control measures. Metabolites are expressed as a concentration in millimoles (mM) per unit tissue volume.
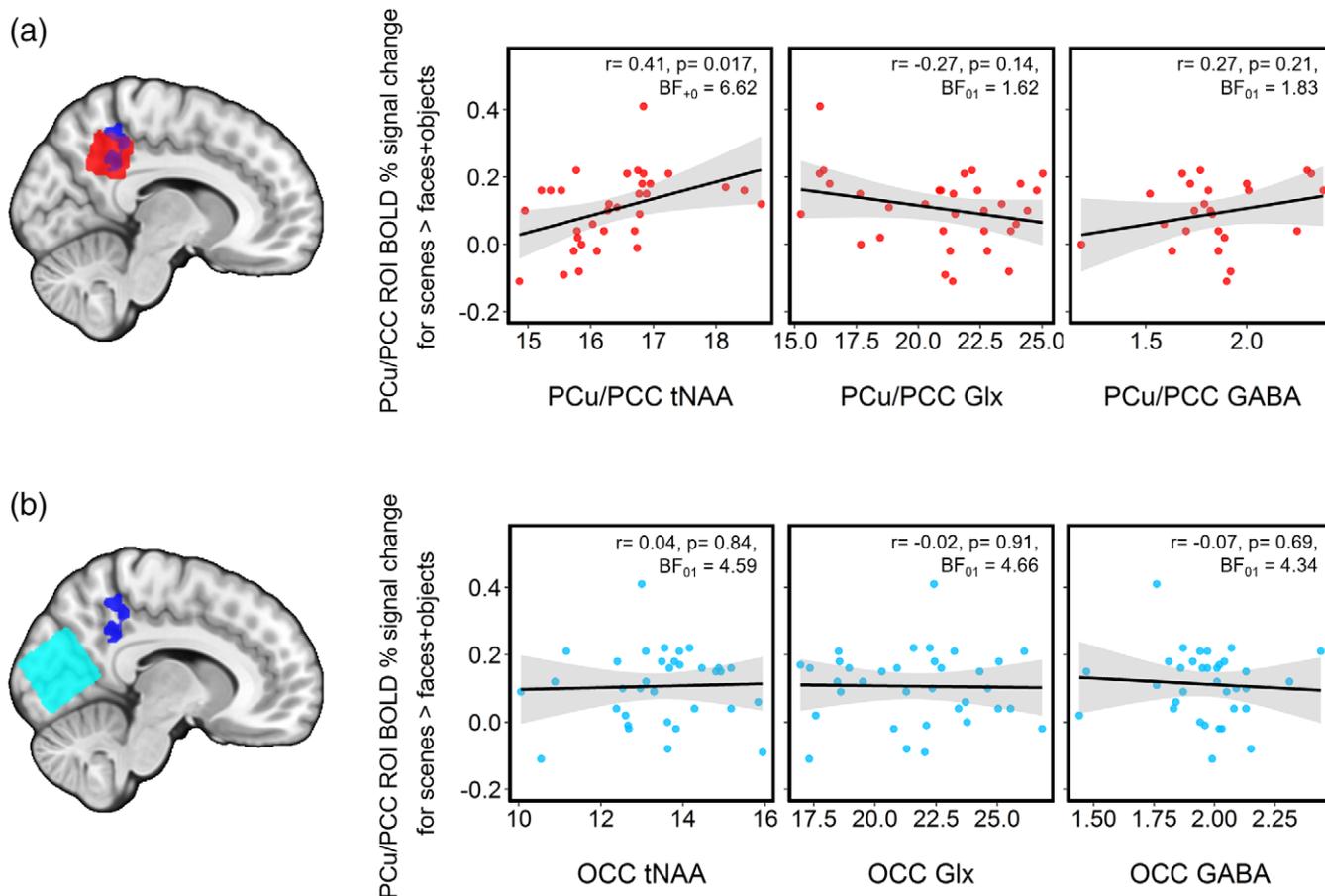
FIGURE 3 Pearson correlations of PCu/PCC ROI BOLD percent signal change for the contrast scenes >faces + objects with each of the three ^{1}H-MRS metabolites from (a) the PCu/PCC MRS voxel (red data points) and (b) the OCC control voxel (blue data points). Metabolites are expressed as a concentration in millimoles (mM) per unit tissue volume. Grey shaded areas show the 95% confidence intervals [Color figure can be viewed at wileyonlinelibrary.com]

each voxel from a single subject. Table 2 gives the mean metabolite concentrations in each voxel, and sample sizes remaining after data exclusions due to ^{1}H-MRS and fMRI data quality assessment, to show data remaining for fMRI-MRS correlations.

3.4 | MRS-fMRI relationships

3.4.1 | Pearson correlation of PCu/PCC ROI BOLD with ^{1}H-MRS metabolites

There was a significant positive correlation between the BOLD percent signal change for scenes > faces + objects in our *a priori* PCu/PCC ROI and the concentration of tNAA in the PCu/PCC ^{1}H-MRS voxel ($r[33] = 0.41$, $p = 0.017$, $BF_{+0} = 6.62$, 95% Bayes CI = 0.09 and 0.65; see Figure 3a). This association remained significant when a Spearman rho correlation, which is robust to univariate outliers (Croux & Dehon, 2010), was performed ($r_s[33] = 0.48$, $p = 0.005$).

This relationship appeared to be regionally selective, as there was no significant correlation between PCu/PCC BOLD for scenes > faces + objects and OCC tNAA ($r[34] = 0.04$, $p = 0.84$, $BF_{01} = 4.59$, 95% Bayes CI = −0.29 and 0.36; see Figure 3b). The difference between correlations for PCu/PCC BOLD for scenes > faces + objects with PCu/PCC tNAA versus with OCC tNAA showed a trend towards being significant ($Z = 1.58$, $p = 0.058$).

There were no significant correlations between PCu/PCC BOLD for scenes > faces + objects and either PCu/PCC Glx ($r[32] = −0.27$, $p = 0.14$, $BF_{01} = 1.62$, 95% Bayes CI = −0.54 and 0.09), or PCu/PCC GABA+ ($r[24] = 0.27$, $p = 0.21$, $BF_{01} = 1.83$, 95% Bayes CI = −0.14 and 0.58; see Figure 3a). There was also no relationship between PCu/PCC BOLD for scenes > faces + objects with OCC Glx ($r[34] = −0.02$, $p = 0.91$, $BF_{01} = 4.66$, 95% Bayes CI = −0.34 and 0.31) or with OCC GABA+ ($r[34] = −0.07$, $p = 0.69$, $BF_{01} = 4.34$, 95% Bayes CI = −0.38 and 0.26; see Figure 3b).

To confirm that the positive correlation identified between the PCu/PCC BOLD response for scenes and PCu/PCC tNAA was indeed driven by *activation* for scenes, rather than *deactivation* for faces and objects relative to scenes (as depicted in Figure 2f), additional correlations were performed between PCu/PCC BOLD for scenes > size baseline and PCu/PCC tNAA or OCC tNAA. Consistent with the above correlations, a significant positive relationship was identified between PCu/PCC BOLD for scenes > size and PCu/PCC tNAA ($r[33] = 0.42$, $p = 0.016$, $BF_{10} = 7.03$, 95% Bayes CI = 0.09 and 0.65). Again, this was regionally selective, as there was no significant correlation between PCu/PCC BOLD for scenes > size with OCC tNAA ($r[34] = 0.09$, $p = 0.63$, $BF_{01} = 4.18$, 95% Bayes CI = −0.25 and 0.40; see Figure 4). The difference between these two correlations showed a trend towards being significant ($Z = 1.41$, $p = 0.079$).
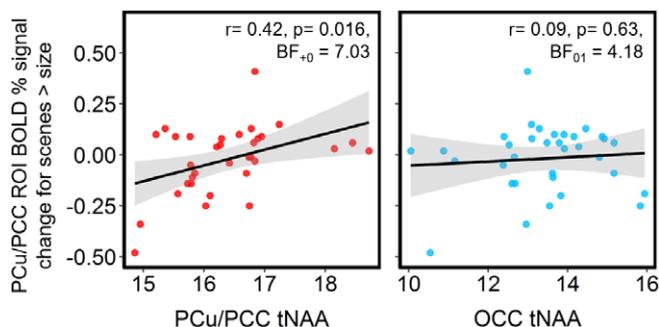
FIGURE 4 Pearson correlations of PCu/PCC ROI BOLD percent signal change for the contrast scenes > size with PCu/PCC or OCC tNAA. Metabolites are expressed as a concentration in millimoles (mM) per unit tissue volume. Grey shaded areas show the 95% confidence intervals [Color figure can be viewed at wileyonlinelibrary.com]

To further assess whether the positive correlation identified between the PCu/PCC BOLD response for scenes and PCu/PCC tNAA was indeed specific to scenes, we tested *posthoc* for any significant correlation between PCu/PCC tNAA and BOLD percent signal change for faces or objects contrasted with the size baseline. There was no significant correlation between either faces > size and tNAA ($r[33]$ = 0.18, p = 0.31, BF_{01} = 2.79, 95% Bayes CI = −0.16 and 0.48) or objects > size with tNAA ($r[33]$ = 0.25, p = 0.16, BF_{01} = 1.81, 95% Bayes CI = −0.10 and 0.53).

To further test the regional specificity of the relationship between scene BOLD and tNAA, we assessed this relationship in an independently defined scene-sensitive OCC ROI. This *posthoc* analysis of OCC BOLD response to scenes > size revealed no significant correlation between OCC BOLD and either OCC tNAA ($r[34]$ = 0.19, p = 0.28, BF_{01} = 2.69, 95% Bayes CI = −0.15 and 0.48) or OCC GABA+ ($r[34]$ = −0.29, p = 0.10, BF_{01} = 1.25, 95% Bayes CI = −0.55 and 0.05).

3.4.2 | Voxel-wise GLM using ^{1}H-MRS as a regressor

The relationship between PCu/PCC tNAA and BOLD for scenes > faces + objects identified above was also identified when PCu/PCC tNAA was used as a regressor in the GLM within the PCu/PCC ^{1}H-MRS voxel mask area (see Figure 5). This revealed a significant cluster of 167 voxels where PCu/PCC tNAA was positively correlated

with the BOLD response to scenes > faces + objects (peak MNI co-ordinate 8, −48, 48; peak Z = 3.76). As depicted in Figure 5, this was located in a highly similar region to the *a priori* PCu/PCC ROI, supporting the selective relationship between PCu/PCC BOLD for scenes and PCu/PCC tNAA concentration.

When Glx or GABA+ were included as regressors in separate GLMs, no significant clusters were identified reflecting positive or negative associations with PCu/PCC BOLD for scenes > faces + objects.

4 | DISCUSSION

We adopted a multimodal functional and biochemical imaging approach to test whether individual differences in PCu/PCC BOLD activity during complex scene discrimination were linked to concentrations of PCu/PCC ^{1}H-MRS metabolites. We found a significant positive correlation between the PCu/PCC BOLD response to scenes and the resting state concentration of tNAA in PCu/PCC. This pattern was not evident with Glx or GABA+ and was regionally specific to PCu/PCC, since OCC tNAA concentrations were not linked with either PCu/PCC or OCC BOLD activity.

The PCu/PCC is a core posterior hub of the DMN (Fransson & Marrelec, 2008; Raichle, 2015; Utevsky et al., 2014). Historically, the DMN was identified as a task-negative network, since it was reliably engaged during passive conditions, including fixation (Raichle et al., 2001). Far from being passive, however, default activity during fixation is hypothesised to reflect spontaneous cognitive processes including autobiographical recall, imagination and prospection, although accounts differ as to the role of PCu/PCC in such processes (Andrews-Hanna et al., 2014; Buckner & Carroll, 2007; Hassabis & Maguire, 2007; Schacter et al., 2012; Spreng, 2012). Here, both the ROI and whole brain analyses revealed that PCu/PCC responded significantly more to scenes than to either faces or objects, a finding inconsistent with a simple task-negative account of PCu/PCC function.

Our finding that dorsal PCu/PCC is particularly involved in complex scene discrimination is, however, consistent with other studies showing a role for activation in this region in a variety of scene-related tasks including scene working memory (Hodgetts et al., 2016); mental scene construction (Hassabis & Maguire, 2007; Palombo, Hayes, Peterson, Keane, & Verfaellie, 2018; Robin et al., 2018); as well as
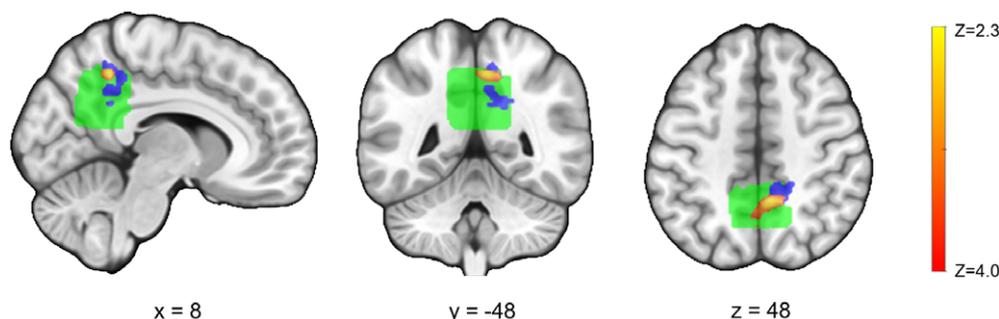

FIGURE 5 Voxel-wise regression analysis rendered on MNI152 standard brain template. Green shows the PCu/PCC ^{1}H-MRS voxel mask area for the tNAA analysis, created by overlaying the participants' PCu/PCC ^{1}H-MRS voxels. Blue shows the *a priori* PCu/PCC mask used in the ROI analysis. Red/yellow shows the significant cluster of 167 voxels within the green ^{1}H-MRS voxel mask area where PCu/PCC tNAA is positively correlated with BOLD for scenes >faces + objects (voxel-wise threshold of Z < 2.3, cluster-wise threshold of p < 0.01 corresponding to clusters >42 voxels) [Color figure can be viewed at wileyonlinelibrary.com]

large-scale spatial navigation in virtual reality environments (Ekstrom, Huffman, & Starrett, 2017). The PCu/PCC region is heavily interconnected with core scene processing regions including retrosplenial and parahippocampal cortices (Hutchison et al., 2014; Kravitz et al., 2011; Parvizi et al., 2006; Passarelli et al., 2018; which were preferentially activated here by scenes alongside PCu/PCC; see also Lee et al., 2008; Hodgetts et al., 2016, 2017), and also links the DMN with the dorsal attention network (Spreng, Sepulcre, Turner, Stevens, & Schacter, 2013), placing it in a key anatomical position to coordinate processes important for scene discrimination performance.

Our fMRI findings thus lend support to accounts in which PCu/PCC contributes to a posteromedial system critical for the construction of mental scenes (Hassabis & Maguire, 2007) or more generally situation models (Murray et al., 2017; Ranganath & Ritchey, 2012), which critically underpin autobiographical memory retrieval, simulation of future episodes, spatial navigation and, as shown here, view-invariant scene perception. Successful performance on scene oddity requires such internal models, because participants must be able to locate each viewpoint (and therefore reject the odd-one-out) within an overarching unified spatial context whose unseen aspects must be internally generated (see also Bar et al., 2007).

4.1 | BOLD-tNAA relationship

A key novel finding from this study was the positive association, across two complementary analysis approaches, between scene-selective PCu/PCC activity and intraregional tNAA concentration. Specifically, where an individual showed a greater PCu/PCC BOLD response for scenes, this was associated with higher tNAA levels. This relationship was specific to scenes, as there were no significant relationships between the PCu/PCC BOLD response to faces or objects with PCu/PCC tNAA. Based on previous studies on tNAA, animal literature, and the proposed functions of tNAA, we offer three potential (albeit speculative) explanations for our scene BOLD and tNAA finding:

1. NAA, which is present predominantly in neuronal cells (Simmons, Frondoza, & Coyle, 1991), is considered as a biomarker of neuronal and axonal density and integrity (Duarte, Lei, Mlynárik, & Gruetter, 2012; Rae, 2014). The positive correlation between tNAA and the local BOLD response, therefore, could indicate that a higher density of neurons that respond to scenes (vs. faces and objects) leads to an increased scene BOLD response.

2. NAA is synthesised in neuronal mitochondria (the site of aerobic respiration to produce ATP; Patel & Clark, 1979), and there is evidence that NAA and mitochondrial function are coupled, as pharmacological inhibition of mitochondrial respiratory chain enzymes required for ATP synthesis are associated with a decrease in NAA (Bates et al., 1996). ATP production is required following neuronal activity to replenish energy stores expended during this energy-demanding process (Logothetis, 2002). The BOLD response is an indirect measure of the increase in nutrients (e.g., oxygen and glucose) delivered to the site of neuronal activity for ATP production. A second possible mechanism linking tNAA with BOLD, therefore, is that a higher BOLD response could represent greater functional

capacity of the neuronal mitochondria to produce ATP, which is associated with levels of NAA.

3. A third possible mechanism is based on NAA being a precursor molecule for N-acetyl-aspartyl-glutamate (NAAG; Moffet et al., 2007; Rae, 2014). In most ^{1}H-MRS studies, NAA and NAAG are combined to create a composite tNAA measure (Rae, 2014). A recent functional ^{1}H-MRS (fMRS) study, however, assessed NAA and NAAG separately, and found that NAAG increases and NAA decreases in concentration following neuronal stimulation (Landim et al., 2016). NAAG induces a vasodilatory response in local blood vessels, via being exported from neurons to astrocytes where it binds to the mGluR3 glutamate receptor. This results in the release of vasoactive agents, which is in turn associated with an increase in the BOLD response (Baslow et al., 2016). Further evidence that NAAG is associated with BOLD comes from the pharmacological inhibition of NAAG breakdown, which causes an increase in the BOLD response for a few minutes (Baslow, Dyakin, Nowak, Hungund, & Guilfoyle, 2005). Returning to the tNAA-BOLD relationship identified here, if there was a higher amount of regional tNAA (i.e., combined NAA and NAAG), there could be more substrate (NAA) to produce more NAAG. In turn, this could result in a greater vasoactive response, reflected in a greater BOLD response. Future (invasive) studies will be required to untangle these possible mechanisms.

Our findings also suggest some regional specificity of the link between BOLD and tNAA, since we found no correlation between OCC tNAA and the OCC response to scenes. This could reflect some unique physiological properties of PCu/PCC and/or tNAA (Dollé et al., 2018). NAA is not distributed homogeneously in the brain, but rather, levels are highly variable among different neuronal types (Moffet et al., 2007). Further work is needed to address this question.

The causes of interindividual variation in tNAA in young adulthood are not fully understood, but likely include a complex interplay between genetic and environmental factors over the lifecourse. Levels of tNAA have been shown to be highly heritable (Batouli et al., 2012), but are also sensitive to early environmental influences, including stress (McLean et al., 2012). Future large scale studies of genetic and environmental influences on PCu/PCC metabolite levels in humans across the lifespan will be required to address this critical question, which may have implications for understanding lifespan influences on cognitive and neural ageing (Dollé et al., 2018; Jagust & Mormino, 2011).

4.2 | BOLD-GABA+ and BOLD-Glx relationships

We found no significant correlation between PCu/PCC BOLD scene activity and regional GABA+ or Glx, which contrasts with a previous study of DMN deactivation (Hu et al., 2013). The lack of BOLD-Glx and BOLD-GABA+ correlations could reflect a lower signal-to-noise ratio for the multiple peaks of Glx and GABA+ which overlap with other metabolites, compared to the large peak of tNAA (Harris et al., 2017; Rae, 2014; Stagg & Rothman, 2014). The data quality for tNAA was also better than that of GABA+, as many more GABA+ than tNAA measurements were excluded

through quality control assessments. Alternatively, differences in sample age might be responsible as our sample was younger on average that than of Hu et al. (2013) (mean age 34.4 ± 8.6 years). Substantial age-related changes have been reported in both PCu/PCC GABA+ concentration and DMN deactivation, even prior to middle age (Gao et al., 2013; Nelson et al., 2016).

More substantively, our lack of significant correlation for scene-task related PCu/PCC BOLD with local GABA+ and Glx could be consistent with accounts that different populations of neurons within posterior DMN have somewhat distinct functions. Single unit recording studies have recently revealed that neural populations in PCu/PCC associated with "default mode" activity (i.e., showing task-negative responses) may be distinct from those involved in active (e.g., mnemonic or scene-construction) processing (Daitch & Parvizi, 2018; Fox et al., 2018). In addition, patterns of DMN network connectivity are somewhat different during rest versus autobiographical memory and future thinking (Bellana, Liu, Diamond, Grady, & Moscovitch, 2017). This might then in turn lead to different neurometabolite correlates of resting (i.e., as in Hu et al., 2013) versus active processing (i.e., scene tasks as in this study) in PCu/PCC. Further fMRI-MRS studies (Ip et al., 2017) will be needed to explore this in more detail.

An alternative, more mechanistic reason could be that BOLD-tNAA and BOLD-GABA+ or BOLD-Glx relationships are capturing quite different physiological processes. For example, GABA+ and Glx could indicate inhibitory and excitatory tone (Farrant & Nusser, 2005; Rae, 2014; Stagg, Bachtiar, & Johansen-Berg, 2011), whereas tNAA could reflect neuro-vascular coupling, as speculated above. In the absence of strong Bayes Factors in support of the null for BOLD-GABA+ and BOLD-Glx relationships; however, these last two possibilities must remain speculative.

4.3 | Limitations

Although ^{1}H-MRS has the advantage that it is the only neuroimaging technique that can contribute knowledge of biochemistry noninvasively *in vivo*, there are limitations to this technique. The large voxel sizes required to quantify metabolites present at very low concentrations limits the spatial resolution that ^{1}H-MRS can provide in comparison to the high spatial resolution of fMRI (Stagg & Rothman, 2014). This is particularly problematic for GABA quantification (Mullins et al., 2014). An attempt was made at reducing the size of the PCu/PCC ^{1}H-MRS voxel from the standard $3 \times 3 \times 3$ cm to $2 \times 2 \times 3$ cm to improve regional specificity in this study; this came; however, at the cost of several PCu/PCC MEGA-PRESS spectra being of too poor quality to use the GABA+ measurement obtained from this region. Moving to stronger magnetic field strengths (e.g., 7 T) could improve signal-to-noise for the metabolite measurements, making it possible to reduce the voxel sizes to improve the spatial resolution of the ^{1}H-MRS measures (Terpstra et al., 2016; Tkáč, Öz, Adriany, Uğurbil, & Gruetter, 2009).

As is common in previous fMRI-MRS studies, a limitation of our approach was that the ^{1}H-MRS and fMRI scans were acquired separately. The concentrations of tNAA, Glx and GABA+ measured, therefore, reflected their concentrations during an unconstrained resting state rather than during the task. Recent fMRI-MRS studies are now attempting to assess task-related ^{1}H-MRS changes, through functional MRS (fMRS; Apšvalka, Gadie, Clemence, & Mullins, 2015; Huang et al., 2015; Landim et al., 2016), or through collecting ^{1}H-MRS and fMRI data simultaneously, by acquiring both within the same TE (Ip et al., 2017). Future studies could assess the relationship between task-evoked changes in tNAA (and other metabolites) and the BOLD response in PCu/PCC during scene discrimination and construction.

The focus of our study was on PCu/PCC, but it would be interesting to extend the work to other scene-processing regions, including parahippocampal cortex and hippocampus, and to other functionally specialised regions. Due to its location and size, it is technically challenging to acquire high quality ^{1}H-MRS spectra in the hippocampal region (Geurts et al., 2004; Kreis, 2004; Venkatraman et al., 2006). Future studies using ultra-high field ^{1}H-MRS (e.g., Voets, Hodgetts, Sen, Adcock, & Emir, 2017) are now required.

We found no significant correlations between either PCu/PCC BOLD or PCu/PCC tNAA and individual differences in task performance. It has been suggested that individual differences in neural engagement should be independent of RTs, whereas differences in neural effort should covary with RTs (Taylor, Rastle, & Davis, 2014). Applied to our findings, higher tNAA in PCu/PCC might lead to greater neural engagement of PCu/PCC in scene processing, without influencing the effort involved in processing scenes. Alternatively, the lack of correlation with performance could reflect high overall performance levels in our young adult sample.

5 | SUMMARY

In conclusion, our multimodal imaging study revealed that dorsal PCu/PCC shows a selective response to scenes compared to faces or objects. This is consistent with the view that this region is a key region in a posteromedial network critical for scene or situation model construction, including in the service of online perception. The magnitude of the PCu/PCC BOLD response to scenes (relative to the other stimulus categories, including low-level baseline) was positively associated with the concentration of the PCu/PCC ^{1}H-MRS metabolite tNAA, and not with concentrations of PCu/PCC GABA+ or Glx, nor with OCC metabolite concentrations. This finding provides novel evidence on the biochemical correlates of PCu/PCC activity, raising the intriguing possibility that neuronal density and/or mitochondrial energy metabolism could underpin individual differences in the magnitude of the scene-selective BOLD response in this key brain hub.

REFERENCES

Andrews-Hanna, J. R., Saxe, R., & Yarkoni, T. (2014). Contributions of episodic retrieval and mentalizing to autobiographical thought: Evidence from functional neuroimaging, resting-state connectivity, and fMRI meta-analyses. *NeuroImage*, *91*, 324–335. https://doi.org/10.1016/j.neuroimage.2014.01.032

Apšvalka, D., Gadie, A., Clemence, M., & Mullins, P. G. (2015). Event-related dynamics of glutamate and BOLD effects measured using functional magnetic resonance spectroscopy (fMRS) at 3 T in a repetition suppression paradigm. *NeuroImage*, *118*, 292–300. https://doi.org/10.1016/j.neuroimage.2015.06.015

Bar, M., Aminoff, E., Mason, M., & Fenske, M. (2007). The units of thought. *Hippocampus*, *17*, 420–428. http://doi.wiley.com/10.1002/hipo.20287

Barense, M. D., Henson, R. N. A., Lee, A. C. H., & Graham, K. S. (2010). Medial temporal lobe activity during complex discrimination of faces, objects, and scenes: Effects of viewpoint. *Hippocampus*, *20*, 389–401.

Baslow, M. H., Cain, C. K., Sears, R., Wilson, D. A., Bachman, A., Gerum, S., & Guilfoyle, D. N. (2016). Stimulation-induced transient changes in neuronal activity, blood flow and N-acetylaspartate content in rat prefrontal cortex: A chemogenetic fMRS-BOLD study. *NMR in Biomedicine*, *29*, 1678–1687. https://doi.org/10.1002/nbm.3629

Baslow, M. H., Dyakin, V. V., Nowak, K. L., Hungund, B. L., & Guilfoyle, D. N. (2005). 2-PMPA, a NAAG peptidase inhibitor, attenuates magnetic resonance BOLD signals in brain of anesthetized mice: Evidence of a link between neuron NAAG release and hyperemia. *Journal of Molecular Neuroscience*, *26*, 001–016. http://link.springer.com/10.1385/JMN:26:1:001.

Bates, T. E., Strangward, M., Keelan, J., Davey, G. P., Munro, P. M., & Clark, J. B. (1996). Inhibition of N-acetylaspartate production: Implications for 1H-MRS studies in vivo. *Neuroreport*, *7*, 1397–1400.

Batouli, S. A. H., Sachdev, P. S., Wen, W., Wright, M. J., Suo, C., Ames, D., & Trollor, J. N. (2012). The heritability of brain metabolites on proton magnetic resonance spectroscopy in older individuals. *NeuroImage*, *62*, 281–289. https://doi.org/10.1016/j.neuroimage.2012.04.043

Batra, N. A., Seres-Mailo, J., Hanstock, C., Seres, P., Khudabux, J., Bellavance, F., … Le Melledo, J.-M. (2008). Proton magnetic resonance spectroscopy measurement of brain glutamate levels in premenstrual Dysphoric disorder. *Biological Psychiatry*, *63*, 1178–1184. https://doi.org/10.1016/j.biopsych.2007.10.007

Beckmann, C. F., Jenkinson, M., & Smith, S. M. (2003). General multilevel linear modeling for group analysis in FMRI. *NeuroImage*, *20*, 1052–1063. https://doi.org/10.1016/S1053-8119(03)00435-X

Bellana, B., Liu, Z.-X., Diamond, N. B., Grady, C. L., & Moscovitch, M. (2017). Similarities and differences in the default mode network across rest, retrieval, and future imagining. *Human Brain Mapping*, *38*, 1155–1171. http://doi.wiley.com/10.1002/hbm.23445

Bottomley, P. A. (1984). Selective volume method for performing localized NMR spectroscopy. US patent 4 480 228.

Buckner, R. L., & Carroll, D. C. (2007). Self-projection and the brain. *Trends in Cognitive Sciences*, *11*, 49–57. https://doi.org/10.1016/j.tics.2006.11.004

Bzdok, D., Heeger, A., Langner, R., Laird, A. R., Fox, P. T., Palomero-Gallagher, N., … Eickhoff, S. B. (2015). Subspecialization in the human posterior medial cortex. *NeuroImage*, *106*, 55–71. https://doi.org/10.1016/j.neuroimage.2014.11.009

Cavassila, S., Deval, S., Huegen, C., van Ormondt, D., & Graveron-Demilly, D. (2001). Cramér-Rao bounds: An evaluation tool for quantitation. *NMR in Biomedicine*, *14*, 278–283. https://doi.org/10.1002/nbm.701

Chan, D., Gallaher, L. M., Moodley, K., Minati, L., Burgess, N., & Hartley, T. (2016). The 4 mountains test: A short test of spatial memory with high sensitivity for the diagnosis of pre-dementia Alzheimer's disease. *Journal of Visualized Experiments*, *116*, e54454. https://doi.org/10.3791/54454

Croux, C., & Dehon, C. (2010). Influence functions of the spearman and Kendall correlation measures. *Stat Methods Appt*, *19*, 497–515. http://link.springer.com/10.1007/s10260-010-0142-z

Daitch, A. L., & Parvizi, J. (2018). Spatial and temporal heterogeneity of neural responses in human posteromedial cortex. *Proceedings of the National Academy of Sciences of the United States of America*, *115*(18), 4785–4790. http://www.pnas.org/lookup/doi/10.1073/pnas.1721714115

De Bondt, T., De Belder, F., Vanhevel, F., Jacquemyn, Y., & Parizel, P. M. (2015). Prefrontal GABA concentration changes in women—Influence of menstrual cycle phase, hormonal contraceptive use, and correlation with premenstrual symptoms. *Brain Research*, *1597*, 129–138. https://doi.org/10.1016/j.brainres.2014.11.051

Dean, H. L. (2006). Allocentric spatial referencing of neuronal activity in macaque posterior cingulate cortex. *The Journal of Neuroscience*, *26*, 1117–1127. https://doi.org/10.1523/JNEUROSCI.2497-05.2006

Deichmann, R., Gottfried, J., Hutton, C., & Turner, R. (2003). Optimized EPI for fMRI studies of the orbitofrontal cortex. *NeuroImage*, *19*, 430–441. https://doi.org/10.1016/S1053-8119(03)00073-9

Diedenhofen, B., & Musch, J. (2015). Cocor: A comprehensive solution for the statistical comparison of correlations. Jake Olivier. *PLoS One*, *10*, e0121945 https://doi.org/10.1371/journal.pone.0121945

Dienes, Z., & Mclatchie, N. (2018). Four reasons to prefer Bayesian analyses over significance testing. *Psychonomic Bulletin & Review*, *25*, 207–218. https://doi.org/10.3758/s13423-017-1266-z

Dollé, J.-P., Rodgers, J. M., Browne, K. D., Troxler, T., Gai, F., & Smith, D. H. (2018). Newfound effect of N-acetylaspartate in preventing and reversing aggregation of amyloid-beta in vitro. *Neurobiology of Disease*, *117*, 161–169. https://linkinghub.elsevier.com/retrieve/pii/S096999611830161X

Duarte, J. M. N., Lei, H., Mlynárik, V., & Gruetter, R. (2012). The neurochemical profile quantified by in vivo 1H NMR spectroscopy. *NeuroImage*, *61*, 342–362. https://doi.org/10.1016/j.neuroimage.2011.12.038

Duncan, N. W., Wiebking, C., Munoz-Torres, Z., & Northoff, G. (2014). How to investigate neuro-biochemical relationships on a regional level in humans? Methodological considerations for combining functional with biochemical imaging. *Journal of Neuroscience Methods*, *221*, 183–188. https://doi.org/10.1016/j.jneumeth.2013.10.011

Duncan, N. W., Wiebking, C., & Northoff, G. (2014). Associations of regional GABA and glutamate with intrinsic and extrinsic neural activity in humans-a review of multimodal imaging studies. *Neuroscience and Biobehavioral Reviews*, *47*, 36–52. http://www.ncbi.nlm.nih.gov/pubmed/25066091

Edden, R. A. E., Puts, N. A. J., Harris, A. D., Barker, P. B., & Evans, C. J. (2014). Gannet: A batch-processing tool for the quantitative analysis of gamma-aminobutyric acid-edited MR spectroscopy spectra. *Journal of Magnetic Resonance Imaging*, *40*, 1445–1452. https://doi.org/10.1002/jmri.24478

Eklund, A., Nichols, T. E., & Knutsson, H. (2016). Cluster failure: Why fMRI inferences for spatial extent have inflated false-positive rates. *Proceedings of the National Academy of Sciences*, *113*, 7900–7905. https://doi.org/10.1073/pnas.1602413113

Ekstrom, A. D., Huffman, D. J., & Starrett, M. (2017). Interacting networks of brain regions underlie human spatial navigation: a review and novel synthesis of the literature. *Journal of Neurophysiology*, *118*, 3328–3344. https://doi.org/10.1152/jn.00531.2017

Enzi, B., Duncan, N. W., Kaufmann, J., Tempelmann, C., Wiebking, C., & Northoff, G. (2012). Glutamate modulates resting state activity in the perigenual anterior cingulate cortex—A combined fMRI–MRS study. *Neuroscience*, *227*, 102–109. https://doi.org/10.1016/j.neuroscience.2012.09.039

Epperson, C. N., Haga, K., Mason, G. F., Sellers, E., Gueorguieva, R., Zhang, W., … Krystal, J. H. (2002). Cortical γ-Aminobutyric acid levels across the menstrual cycle in healthy women and those with premenstrual Dysphoric disorder. *Archives of General Psychiatry*, *59*, 851–858. https://doi.org/10.1001/archpsyc.59.9.851

Farrant, M., & Nusser, Z. (2005). Variations on an inhibitory theme: Phasic and tonic activation of GABAA receptors. *Nature Reviews. Neuroscience*, *6*, 215–229. https://doi.org/10.1038/nrn1625

Fox, K. C. R., Foster, B. L., Kucyi, A., Daitch, A. L., & Parvizi, J. (2018). Intracranial electrophysiology of the human default network. *Trends in Cognitive Sciences*, *22*, 307–324. https://doi.org/10.1016/j.tics.2018.02.002

Fransson, P., & Marrelec, G. (2008). The precuneus/posterior cingulate cortex plays a pivotal role in the default mode network: Evidence from a partial correlation network analysis. *NeuroImage*, *42*, 1178–1184. https://doi.org/10.1016/j.neuroimage.2008.05.059

Futamura, A., Honma, M., Shiromaru, A., Kuroda, T., Masaoka, Y., Midorikawa, A., … Ono, K. (2018). Singular case of the driving instructor: Temporal and topographical disorientation. *Neurology and Clinical Neuroscience*, *6*, 16–18. https://doi.org/10.1111/ncn3.12166

Gao, F., Edden R a, E., Li, M., Puts N a, J., Wang, G., Liu, C., ... Barker, P. B. (2013). Edited magnetic resonance spectroscopy detects an age-related decline in brain GABA levels. *NeuroImage*, 78, 75–82. http://www.pubmedcentral.nih.gov/articlerender.fcgi?artid=3716005&tool=pmcentrez&rendertype=abstract

Geurts, J. J. G., Barkhof, F., Ja, C., Uitdehaag, B. M. J., Polman, C. H., & Pouwels, P. J. W. (2004). Quantitative 1H-MRS of healthy human cortex, hippocampus, and thalamus: Metabolite concentrations, quantification precision, and reproducibility. *Journal of Magnetic Resonance Imaging*, 20, 366–371. http://www.ncbi.nlm.nih.gov/pubmed/15332241

Greenhouse, I., Noah, S., Maddock, R. J., & Ivry, R. B. (2016). Individual differences in GABA content are reliable but are not uniform across the human cortex. *NeuroImage*, 139, 1–7. https://doi.org/10.1016/j.neuroimage.2016.06.007

Hancu, I. (2009). Optimized glutamate detection at 3T. *Journal of Magnetic Resonance Imaging*, 30, 1155–1162. https://doi.org/10.1002/jmri.21936

Hao, X., Xu, D., Bansal, R., Dong, Z., Liu, J., Wang, Z., ... Peterson, B. S. (2013). Multimodal magnetic resonance imaging: The coordinated use of multiple, mutually informative probes to understand brain structure and function. *Human Brain Mapping*, 34, 253–271. https://doi.org/10.1002/hbm.21440

Harris, A. D., Puts, N. A. J., Anderson, B. A., Yantis, S., Pekar, J. J., Barker, P. B., & Edden, R. A. E. (2015). Multi-regional investigation of the relationship between functional MRI blood oxygenation level dependent (BOLD) activation and GABA concentration. Xi Luo. *PLoS One*, 10, e0117531 https://doi.org/10.1371/journal.pone.0117531

Harris, A. D., Puts, N. A. J., & Edden, R. A. E. (2015). Tissue correction for GABA-edited MRS: Considerations of voxel composition, tissue segmentation, and tissue relaxations. *Journal of Magnetic Resonance Imaging*, 42, 1431–1440. https://doi.org/10.1002/jmri.24903

Harris, A. D., Saleh, M. G., & Edden, R. A. E. (2017). Edited 1 H magnetic resonance spectroscopy in vivo: Methods and metabolites. *Magnetic Resonance in Medicine*, 77, 1377–1389. https://doi.org/10.1002/mrm.26619

Hassabis, D., & Maguire, E. A. (2007). Deconstructing episodic memory with construction. *Trends in Cognitive Sciences*, 11, 299–306. https://doi.org/10.1016/j.tics.2007.05.001

Hodgetts, C. J., Postans, M., Shine, J. P., Jones, D. K., Lawrence, A. D., & Graham, K. S. (2015). Dissociable roles of the inferior longitudinal fasciculus and fornix in face and place perception. *eLife*, 4, 1–25. https://doi.org/10.7554/eLife.07902.001

Hodgetts, C. J., Shine, J. P., Lawrence, A. D., Downing, P. E., & Graham, K. S. (2016). Evidencing a place for the hippocampus within the core scene processing network. *Human Brain Mapping*, 37, 3779–3794. https://doi.org/10.1002/hbm.23275

Hodgetts, C. J., Voets, N. L., Thomas, A. G., Clare, S., Lawrence, A. D., & Graham, K. S. (2017). Ultra-high-field fMRI reveals a role for the Subiculum in scene perceptual discrimination. *The Journal of Neuroscience*, 37, 3150–3159. https://doi.org/10.1523/JNEUROSCI.3225-16.2017

Hu, Y., Chen, X., Gu, H., & Yang, Y. (2013). Resting-state glutamate and GABA concentrations predict task-induced deactivation in the default mode network. *The Journal of Neuroscience*, 33, 18566–18573. https://doi.org/10.1523/JNEUROSCI.1973-13.2013

Huang, Z., Davis, H. H. I. V., Yue, Q., Wiebking, C., Duncan, N. W., Zhang, J., ... Northoff, G. (2015). Increase in glutamate/glutamine concentration in the medial prefrontal cortex during mental imagery: A combined functional mrs and fMRI study. *Human Brain Mapping*, 36, 3204–3212. http://doi.wiley.com/10.1002/hbm.22841

Hutchison, R. M., Culham, J. C., Everling, S., Flanagan, J. R., & Gallivan, J. P. (2014). Distinct and distributed functional connectivity patterns across cortex reflect the domain-specific constraints of object, face, scene, body, and tool category-selective modules in the ventral visual pathway. *NeuroImage*, 96, 216–236. https://doi.org/10.1016/j.neuroimage.2014.03.068

Ip, I. B., Berrington, A., Hess, A. T., Parker, A. J., Emir, U. E., & Bridge, H. (2017). Combined fMRI-MRS acquires simultaneous glutamate and BOLD-fMRI signals in the human brain. *NeuroImage*, 155, 113–119. https://doi.org/10.1016/j.neuroimage.2017.04.030

Irish, M., Halena, S., Kamminga, J., Tu, S., Hornberger, M., & Hodges, J. R. (2015). Scene construction impairments in Alzheimer's disease––A

unique role for the posterior cingulate cortex. *Cortex*, 73, 10–23. https://doi.org/10.1016/j.cortex.2015.08.004

Jagust, W. J., & Mormino, E. C. (2011). Lifespan brain activity, β-amyloid, and Alzheimer's disease. *Trends in Cognitive Sciences*, 15, 520–526. https://doi.org/10.1016/j.tics.2011.09.004.

Jarosz, A. F., & Wiley, J. (2014). What are the odds ? A practical guide to computing and reporting Bayes factors. *The Journal of Problem Solving*, 7, 2–9. https://doi.org/10.7771/1932-6246.1167

Jenkinson, M. (2003). Fast, automated, N-dimensional phase-unwrapping algorithm. *Magnetic Resonance in Medicine*, 49, 193–197. https://doi.org/10.1002/mrm.10354

Jenkinson, M., Bannister, P., Brady, M., & Smith, S. (2002). Improved optimization for the robust and accurate linear registration and motion correction of brain images. *NeuroImage*, 17, 825–841. https://doi.org/10.1006/nimg.2002.1132

Kravitz, D. J., Saleem, K. S., Baker, C. I., & Mishkin, M. (2011). A new neural framework for visuospatial processing. *Nature Reviews. Neuroscience*, 12, 217–230. https://doi.org/10.1038/nrn3008

Kreis, R. (2004). Issues of spectral quality in clinical 1H-magnetic resonance spectroscopy and a gallery of artifacts. *NMR in Biomedicine*, 17, 361–381. http://doi.wiley.com/10.1002/nbm.891

Kriegeskorte, N., Simmons, W. K., Bellgowan, P. S. F., & Baker, C. I. (2009). Circular analysis in systems neuroscience: The dangers of double dipping. *Nature Neuroscience*, 12, 535–540. https://doi.org/10.1038/nn.2303

Landim, R. C. G., Edden, R. A. E., Foerster, B., Li, L. M., Covolan, R. J. M., & Castellano, G. (2016). Investigation of NAA and NAAG dynamics underlying visual stimulation using MEGA-PRESS in a functional MRS experiment. *Magnetic Resonance Imaging*, 34, 239–245. https://doi.org/10.1016/j.mri.2015.10.038

Lee, A. C. H., Scahill, V. L., & Graham, K. S. (2008). Activating the medial temporal lobe during oddity judgment for faces and scenes. *Cerebral Cortex*, 18, 683–696.

Leech, R., & Sharp, D. J. (2014). The role of the posterior cingulate cortex in cognition and disease. *Brain*, 137, 12–32. https://doi.org/10.1093/brain/awt162

Lipp, I., Evans, C. J., Lewis, C., Murphy, K., Wise, R. G., & Caseras, X. (2015). The relationship between fearfulness, GABA+, and fear-related BOLD responses in the insula. Ed. Alexandra Kavushansky. *PLoS One*, 10, e0120101 https://doi.org/10.1371/journal.pone.0120101

Logothetis, N. K. (2002). The neural basis of the blood-oxygen-level-dependent functional magnetic resonance imaging signal. *Philosophical Transactions of the Royal Society B*, 357, 1003–1037. https://doi.org/10.1098/rstb.2002.1114

Marsman, M., & Wagenmakers, E. J. (2017). Bayesian benefits with JASP. *The European Journal of Developmental Psychology*, 14, 545–555. https://doi.org/10.1080/17405629.2016.1259614

McLean, J., Krishnadas, R., Batty, G. D., Burns, H., Deans, K. A., Ford, I., ... Cavanagh, J. (2012). Early life socioeconomic status, chronic physiological stress and hippocampal N-acetyl aspartate concentrations. *Behavioural Brain Research*, 235, 225–230. https://doi.org/10.1016/j.bbr.2012.08.013.

Mescher, M., Merkle, H., Kirsch, J., Garwood, M., & Gruetter, R. (1998). Simultaneous in vivo spectral editing and water suppression. *NMR in Biomedicine*, 11, 266–272. https://doi.org/10.1002/(SICI)1099-1492(199810)11:6%3C266::AID-NBM530%3E3.0.CO;2-J

Moffet, J., Ross, B., Arun, P., Madhavarao, C., & Namboodiri, A. (2007). N-Acetylaspartate in the CNS: From neurodiagnostics to neurobiology. *Progress in Neurobiology*, 81, 89–131. https://doi.org/10.1016/j.pneurobio.2006.12.003

Mullins, P. G., McGonigle, D. J., O'Gorman, R. L., Puts, N. A. J., Vidyasagar, R., Evans, C. J., & Edden, R. A. E. (2014). Current practice in the use of MEGA-PRESS spectroscopy for the detection of GABA. *NeuroImage*, 86, 43–52. https://doi.org/10.1016/j.neuroimage.2012.12.004

Murray, E. A., Wise, S. P., & Graham, K. S. (2017). Representational specializations of the hippocampus in phylogenetic perspective. *Neuroscience Letters*, 680, 4–12. https://doi.org/10.1016/j.neulet.2017.04.065. https://doi.org/10.1016/j.neulet.2017.04.065

Nakagawa, S. (2004). A farewell to Bonferroni: The problems of low statistical power and publication bias. *Behavioral Ecology*, 15, 1044–1045. https://doi.org/10.1093/beheco/arh107

Nelson, S. M., Savalia, N. K., Fishell, A. K., Gilmore, A. W., Zou, F., Balota, D. A., & McDermott, K. B. (2016). Default mode network activity predicts early memory decline in healthy young adults aged 18–31. *Cerebral Cortex*, *26*, 3379–3389. https://academic.oup.com/cercor/article-lookup/doi/10.1093/cercor/bhv165

Northoff, G., Walter, M., Schulte, R. F., Beck, J., Dydak, U., Henning, A., ... Boesiger, P. (2007). GABA concentrations in the human anterior cingulate cortex predict negative BOLD responses in fMRI. *Nature Neuroscience*, *10*, 1515–1517. http://www.ncbi.nlm.nih.gov/pubmed/17982452

Palombo, D. J., Hayes, S. M., Peterson, K. M., Keane, M. M., & Verfaellie, M. (2018). Medial temporal lobe contributions to episodic future thinking: Scene construction or future projection? *Cerebral Cortex*, *28*, 447–458. https://doi.org/10.1093/cercor/bhw381

Parvizi, J., Van Hoesen, G. W., Buckwalter, J., & Damasio, A. (2006). Neural connections of the posteromedial cortex in the macaque. *Proceedings of the National Academy of Sciences*, *103*, 1563–1568. https://doi.org/10.1073/pnas.0507729103

Passarelli, L., Rosa, M. G. P., Bakola, S., Gamberini, M., Worthy, K. H., Fattori, P., & Galletti, C. (2018). Uniformity and diversity of cortical projections to Precuneate areas in the macaque monkey: What defines area PGm? *Cerebral Cortex*, *28*, 1700–1717. https://doi.org/10.1093/cercor/bhx067

Patel, T. B., & Clark, J. B. (1979). Synthesis of N-acetyl-l-aspartate by rat brain mitochondria and its involvement in mitochondrial/cytosolic carbon transport. *The Biochemical Journal*, *184*, 539–546.

Rae, C. D. (2014). A guide to the metabolic pathways and function of metabolites observed in human brain 1H magnetic resonance spectra. *Neurochemical Research*, *39*, 1–36. https://doi.org/10.1007/s11064-013-1199-5

Raichle, M. E. (2015). The Brain's default mode network. *Annual Review of Neuroscience*, *38*, 433–447. https://doi.org/10.1146/annurev-neuro-071013-014030

Raichle, M. E., MacLeod, A. M., Snyder, A. Z., Powers, W. J., Gusnard, D. A., & Shulman, G. L. (2001). A default mode of brain function. *Proceedings of the National Academy of Sciences of the United States of America*, *98*, 676–682. https://doi.org/10.1073/pnas.98.2.676

Ranganath, C., & Ritchey, M. (2012). Two cortical systems for memory-guided behaviour. *Nature Reviews. Neuroscience*, *13*, 713–726. https://doi.org/10.1038/nrn3338

Robin, J., Buchsbaum, B. R., & Moscovitch, M. (2018). The primacy of spatial context in the neural representation of events. *The Journal of Neuroscience*, *38*, 2755–2765. http://www.jneurosci.org/lookup/doi/10.1523/JNEUROSCI.1638-17.2018

Sato, N., Sakata, H., Tanaka, Y. L., & Taira, M. (2010). Context-dependent place-selective responses of the neurons in the medial parietal region of macaque monkeys. *Cerebral Cortex*, *20*, 846–858. https://doi.org/10.1093/cercor/bhp147

Schacter, D. L., Addis, D. R., Hassabis, D., Martin, V. C., Spreng, R. N., & Szpunar, K. K. (2012). The future of memory: Remembering, imagining, and the brain. *Neuron*, *76*, 677–694. https://doi.org/10.1016/j.neuron.2012.11.001

Shine, J. P., Hodgetts, C. J., Postans, M., Lawrence, A. D., & Graham, K. S. (2015). APOE-ε4 selectively modulates posteromedial cortex activity during scene perception and short-term memory in young healthy adults. *Scientific Reports*, *5*, 16322. https://doi.org/10.1038/srep16322

Simmons, M. L., Frondoza, C. G., & Coyle, J. T. (1991). Immunocytochemical localization of N-acetyl-aspartate with monoclonal antibodies. *Neuroscience*, *45*, 37–45.

Smith, S. M. (2002). Fast robust automated brain extraction. *Human Brain Mapping*, *17*, 143–155. https://doi.org/10.1002/hbm.10062

Spreng, R. N. (2012). The fallacy of a "task-negative" network. *Frontiers in Psychology*, *3*, 145. https://doi.org/10.3389/fpsyg.2012.00145

Spreng, R. N., Mar, R. A., & Kim, A. S. N. (2009). The common neural basis of autobiographical memory, prospection, navigation, theory of mind, and the default mode: A quantitative meta-analysis. *Journal of Cognitive Neuroscience*, *21*, 489–510. https://doi.org/10.1162/jocn.2008.21029

Spreng, R. N., Sepulcre, J., Turner, G. R., Stevens, W. D., & Schacter, D. L. (2013). Intrinsic architecture underlying the relations among the default, dorsal attention, and Frontoparietal control networks of the human brain. *Journal of Cognitive Neuroscience*, *25*, 74–86. https://doi.org/10.1162/jocn_a_00281

Stagg, C. J., Bachtiar, V., & Johansen-Berg, H. (2011). The role of GABA in human motor learning. *Current Biology*, *21*, 480–484. https://doi.org/10.1016/j.cub.2011.01.069

Stagg, C. J., & Rothman, D. L. (Eds.). (2014). *Magnetic Resonance Spectroscopy: Tools for Neurosceicne Research and Emerging Clinical Applications*. Amsterdam, the Netherlands: Elsevier/Academic Press.

Suzuki, K., Yamadori, A., Hayakawa, Y., & Fujii, T. (1998). Pure topographical disorientation related to dysfunction of the viewpoint dependent visual system. *Cortex*, *34*, 589–599. https://doi.org/10.1016/S0010-9452(08)70516-1

Taylor, J. S. H., Rastle, K., & Davis, M. H. (2014). Interpreting response time effects in functional imaging studies. *NeuroImage*, *99*, 419–433. https://doi.org/10.1016/j.neuroimage.2014.05.073

Terpstra, M., Cheong, I., Lyu, T., Deelchand, D. K., Emir, U. E., Bednařík, P., ... Öz, G. (2016). Test-retest reproducibility of neurochemical profiles with short-echo, single-voxel MR spectroscopy at 3T and 7T. *Magnetic Resonance in Medicine*, *76*, 1083–1091. https://doi.org/10.1002/mrm.26022

Tkáč, I., Öz, G., Adriany, G., Uğurbil, K., & Gruetter, R. (2009). In vivo 1 H NMR spectroscopy of the human brain at high magnetic fields: Metabolite quantification at 4T vs. 7T. *Magnetic Resonance in Medicine*, *62*, 868–879. https://doi.org/10.1002/mrm.22086

Utevsky, A. V., Smith, D. V., & S a, H. (2014). Precuneus is a functional Core of the default-mode network. *The Journal of Neuroscience*, *34*, 932–940. https://doi.org/10.1523/JNEUROSCI.4227-13.2014

van den Heuvel, M. P., & Sporns, O. (2013). Network hubs in the human brain. *Trends in Cognitive Sciences*, *17*, 683–696. https://doi.org/10.1016/j.tics.2013.09.012

Venkatraman, T. N., Hamer, R. M., Perkins, D. O., Song, A. W., Lieberman, J. A., & Steen, R. G. (2006). Single-voxel 1H PRESS at 4.0 T: Precision and variability of measurements in anterior cingulate and hippocampus. *NMR in Biomedicine*, *19*, 484–491. http://doi.wiley.com/10.1002/nbm.1055

Voets, N. L., Hodgetts, C. J., Sen, A., Adcock, J. E., & Emir, U. (2017). Hippocampal MRS and subfield volumetry at 7T detects dysfunction not specific to seizure focus. *Scientific Reports*, *7*(1), 16138–16114. https://doi.org/10.1038/s41598-017-16046-5

Wetzels, R., & Wagenmakers, E.-J. (2012). A default Bayesian hypothesis test for correlations and partial correlations. *Psychonomic Bulletin & Review*, *19*, 1057–1064. https://doi.org/10.3758/s13423-012-0295-x

Wilson, M., Reynolds, G., R a, K., Arvanitis, T. N., & Peet, A. C. (2011). A constrained least-squares approach to the automated quantitation of in vivo 1 H magnetic resonance spectroscopy data. *Magnetic Resonance in Medicine*, *65*, 1–12. https://doi.org/10.1002/mrm.22579

Woolrich, M. W., Behrens, T. E. J., Beckmann, C. F., Jenkinson, M., & Smith, S. M. (2004). Multilevel linear modelling for FMRI group analysis using Bayesian inference. *NeuroImage*, *21*, 1732–1747. https://doi.org/10.1016/j.neuroimage.2003.12.023

Yarkoni, T., Poldrack, R. A., Nichols, T. E., Van Essen, D. C., & Wager, T. D. (2011). Large-scale automated synthesis of human functional neuroimaging data. *Nature Methods*, *8*, 665–670. http://www.nature.com/articles/nmeth1635

Zeidman, P., & Maguire, E. A. (2016). Anterior hippocampus: The anatomy of perception, imagination and episodic memory. *Nature Reviews. Neuroscience*, *17*, 173–182. https://doi.org/10.1038/nrn.2015.24

Zhang, Y., Brady, M., & Smith, S. (2001). Segmentation of brain MR images through a hidden Markov random field model and the expectation-maximization algorithm. *IEEE Transactions on Medical Imaging*, *20*, 45–57. https://doi.org/10.1109/42.906424